Evaluation of corrosion resistance of Al-10Si-Mg alloy obtained by means of Direct Metal Laser Sintering

Marina Cabrini, Sergio Lorenzi, Tommaso Pastore, Simone Pellegrini,*
University of Bergamo, Department of Engineering and Applied Science
Viale Marconi, 5 - 24044 Dalmine (BG), Italy
*Fax 0039 035 2052077 – *marina.cabrini@unibg.it*

Diego Manfredi
Center for Space Human Robotics @Polito, Istituto Italiano di Tecnologia
Turin, Italy

Paolo Fino, Sara Biamino, Claudio Badini
Polytechnic of Turin, Department of Applied Science and Technologies, Turin, Italy

Abstract

Direct Metal Laser Sintering (DMLS) is a powder-bed based Additive Manufacturing (AM) technique, which allows fully dense near net-shape parts to be obtained thanks to a powerful laser source able to melt and consolidate the powders layer by layer. Many types of metals are available for DMLS, and aluminium alloys play a major part in applications in different fields, from aerospace to automotive and robotics, due to their high strength-to-weight ratio. In previous years the DMLS technique has been refined with the final aim of producing complex shape components with these alloys. In this study the corrosion behaviour of an aluminium alloy processed through DMLS was studied using Potentiodynamic (PD) tests and Electrochemical Impedance Spectroscopy (EIS) tests. All the tests were executed on Al-10Si-Mg alloy in aerated diluted Harrison solution on surfaces obtained sectioning samples along different orientations with respect to the building direction. The effect of different surface finishing - shot peening and mechanical polishing - was also evaluated.
The results highlighted preferential dissolution of α-Al at the border of the laser scan tracks and a slight variation with plane orientation. Moreover, the modification of the surface by shot peening or polishing increases pitting potential and reduces corrosion rate.

Keywords

Aluminium silicon magnesium alloy, Direct Metal Laser Sintering (DMLS), Additive Manufacturing (AM), Corrosion, Surface finishing

Abbreviations

AM	Additive Manufacturing
DMLS	Direct Metal Laser Sintering
SLM	Selective Laser Melting
PD	Potentiodynamic
EIS	Electrochemical Impedance Spectroscopy
SEM	Scanning Electron Microscope
AR	As Received
SP	Shot Peened
P	Polished with emery paper and 0.1 μm alumina
SCE	Standard Calomel Reference Electrode

HAZ Heat Affected Zone

Nomenclature

E_{cor}	Corrosion Potential (V vs SCE)
E_{pit}	Pitting Potential (V vs SCE)
i	Current Density ($\mu A/cm^2$)
|Z|	Module (Ωcm^2)

1 Introduction

The characteristic properties of aluminium, such as high strength and stiffness to weight ratio, good formability, good corrosion resistance, and recycling potential make it an ideal candidate to replace heavier materials (steel or copper) in the transport industry. The use of aluminium reduces the weight leading to more fuel-efficient vehicles, lower energy consumption and less air pollution (Miller et al. 2000). Moreover, there is a strong interest in new near-net-shape manufacturing technologies that produce metal components close to the final size and shape, thus requiring only a minimum amount of finishing process. In comparison with traditional processes, additive manufacturing (AM) technologies offer significant benefits, such as near-net-shape capabilities, superior design and geometrical flexibility, reduced tooling and fixturing, shorter cycle time for design and manufacturing, as well as material, energy and cost efficiency. In particular Direct Metal Laser Sintering (DMLS), the trade name of EOS GmbH to indicate the Selective Laser Melting (SLM) process, is an AM technology for the fabrication of dense metallic parts directly from computer-aided design data by melting together different layers of powdered metal with an high power laser source (Manfredi et al. 2013). The components produced are near-net-shape and fit for end-user products. The use of DMLS provides design and manufacturing freedom without the restrictions of traditional forming or machining processes, with the added benefit of lighter components.
On the other hand, DMLS produces a large amount of residual stresses, due to the high thermal gradients inherently present in the process, which if not relieved, could lead to component distortion and dimensional inaccuracy (Shiomi et al. 2004). Mercelis and Kruth pointed out the possibility of having cracks or disconnection of parts from the base plate and suggested heating the substrate plate (Mercelis & Kruth 2006). Additionally, in DMLS, the temperature distribution in the powder bed and consolidated layers changes quickly with time and space. The temperature of the powder particles is elevated rapidly under the action of absorbed energy, causing a molten pool, when the temperature exceeds the melting temperature, and heat affected zones in the surrounding loose powder (Zaeh M et al. 2010). Moreover, despite progress in material flexibility and mechanical performances, relatively poor surface finish still presents a major limitation in the DMLS process: the laser welding process causes a general surface roughness due to partially molten powder and droplets on the surface of the part, which may affect its mechanical, chemical and functional properties (Sun et al. 2014).
In previous studies, Manfredi et al (Manfredi et al. 2013) demonstrated that Al-10Si-Mg alloy specimens obtained by means of DMLS have higher hardness and yield strength than conventional casted specimens in a similar alloy (A360), due to the very fine microstructure and fine distribution of the silicon phase promoted by the extremely rapid cooling and solidification, as also reported by Thijs et al. (Thijs et al. 2013). Furthermore, Manfredi et al. (Manfredi et al. 2014) report a probable presence of Mg_2Si intermetallic at a nanometric scale, as previously observed by Olakanmi et al. (Olakanmi 2013). N. Read et al also observed the increase in the tensile strength of AlSi10Mg compared to die cast A360, in both building directions (Read et al. 2015).
To the best knowledge of the authors, there is a lack of data showing the corrosion behaviour of DMLS aluminium alloys. However, the effect of DMLS can be hypothesized because it produces different microstructures with respect to traditional processes. The role of second phases on the corrosion behaviour of aluminium is generally recognized (Szklarska-Smialowska 1999). The intermetallics containing Cu and Fe are cathodic with respect to the matrix and promote dissolution

of the matrix, while the intermetallics rich in Mg are anodic with respect to the matrix and dissolve preferentially (Wei et al. 1998). Coarse intermetallic Al–Si–Mg-containing particles are strongly reactive in 1 M NaCl solution and seem to be nucleation sites for pits and consequently for intergranular corrosion (Guillaumin et al. 2000). The effect of second phases was also analysed in different alloys by means of Kelvin microprobe by L.E. Fratila-Apachitei et al. on AlSi(Cu) alloy (Fratila-Apachitei et al. 2006) and Andreatta et al on 7xxx alloy (Andreatta et al. 2003). Büchler et al characterized the effect of inclusions using fluorescence microscopy on traditional alloys (Büchler et al. 2000).
However, the aim of this work is to begin recovering this gap thus starting to experimentally investigate the corrosion behaviour DMLS aluminium alloys with particular attention to understand the role of the surface finishing and the anisotropy of DMLS microstructure. In particular in this paper we report the study of Al-10Si-Mg alloy produced by DMLS in Harrison solution which is commonly used for evaluating the corrosion resistance of aluminium alloys (Battocchi et al. 2006). Potentiodynamic (PD) tests and Electrochemical Impedance Spectroscopy (EIS) were performed in aerated diluted Harrison's solution, adopting different surface finishing, both on surfaces parallel and perpendicular to the orientation of building plane, in order to analyse the effect of different textures.

2 Experimental

2.1 Material and specimens

The tests were carried out on specimens obtained by DMLS using a gas atomized Al-10Si-Mg powder produced by EOS (Germany). The alloy composition is reported in Table 1.

Elements	Si	Fe	Cu	Mn	Mg	Zn	Ti	Al
%wt	10.08	0.16	0.001	0.002	0.35	0.002	0.01	bulk

Table 1: chemical composition of the Al Si10Mg powder

This alloy is commonly used in casting due to its near Al-Si eutectic composition and low melting temperature, around 570°C (Davis 1998), (Fulcher, Leigh & Watt 2014). As shown in the scanning electron microscope (SEM) images of Figure 1, the particles have a regular spherical shape, with a diameter ranging from 0.5 to 40 µm, and a mean size of 25 µm.

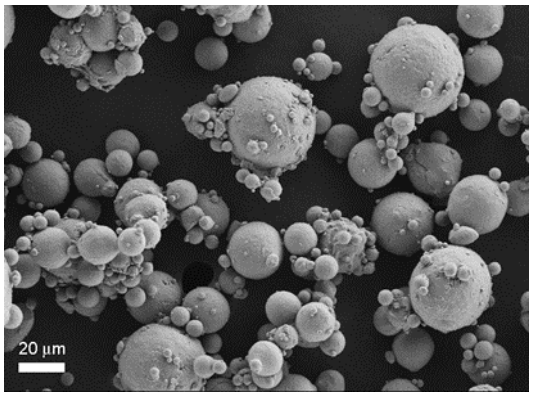

Figure 1: SEM image of the AlSi10Mg powders employed in this study

Specimens to be analysed are disks of 15 mm diameter and 5 mm height. They were fabricated using an EOSINT M270 Xtended machine along different geometric orientations compared to the building platform (xy-plane) and the building direction (z-axis). The specimens with the base circular face on xy-plane were named XY; the specimens with the base face perpendicular to the xy-plane were called XZ (Figure 2).

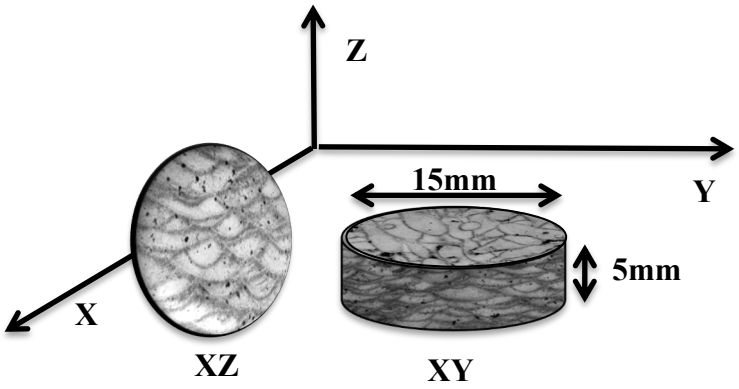

Figure 2: schematic representation of the directions of the production of test specimens

In this machine, a powerful ytterbium fiber laser system in an argon atmosphere is used to melt powders with a continuous power up to 200 W. The detail of the DMLS process, together with the choice of the process parameters to obtain a part with the highest density and the best surface finishing for the Al-10Si-Mg alloy, were described in an earlier study (Manfredi et al. 2013). Then for each orientation, three different surface conditions were considered: the rough surface produced by DMLS (AR) and after shot peening (SP) or polishing with emery paper and 0.1 µm alumina (P). Shot peening treatment was adopted to remove sticky powder not melted and to reduce the superficial roughness as demonstrated in another study by Calignano et al (Calignano et al. 2013). This post-process is a mechanical surface treatment whereby ceramic microspheres impinge on the surface of the component. It is fundamental that shot-peening method is optimized in terms of pressure and time to improve the depth of favourable compressive residual stress fields while minimizing surface roughening: in this study glass microspheres with a diameter comprised between 100-200 µm were used under a pressure of 8 bar for 30 s for each sample. Considering the polished specimens, they were passivated in air for 2 hours before tests. All specimens were degreased in acetone.

2.2 Metallographic examination

The microstructure of specimens was observed at the optical microscope and scanning electron microscope (SEM) with EDS microprobe. The disks were polished without encapsulation in epoxy resin along the circular face. The surface was sequentially grinded using a rotary polisher and SiC abrasive papers up to 4000 grit immersed in water, and finished using 0.1 µm alumina aqueous suspension. The specimens were rinsed with distillate water and acetone in an ultrasonic bath and air-dried between each grinding/polishing step. Specimens were etched using Keller's reagent (1 cm^3 HF, 1.5 cm^3 HCl, 2.5 cm^3 HNO_3, 95 cm^3 H_2O) for 12s.
The optical observations were carried out using a Nikon metallographic microscope and a Zeiss EVO 40 scanning electron microscope. The SEM observation at high magnification were carried out using 20kV acceleration voltage, 200 pA probe current and working distance of 5 mm. The EDS analysis was carried out by means of Oxford Energy Dispersive X-Ray microprobe, using 20kV acceleration voltage, 1000 pA probe current and 8 mm working distance.

2.3 Corrosion tests

The electrochemical tests were performed in one liter ASTM G5 standard cell by using a sample holder with exposure area of 1 cm^2, a standard calomel reference electrode (SCE) and two graphite counter electrodes. Potentiodynamic tests were carried out at 1 mV/s scan rate from -50mV with respect to free corrosion potential (E_{cor}) until the anodic current density reaches 10 mA/cm^2. Before tests, the open circuit potential was monitored for 30 minutes to attain stable values of free corrosion potential. Corrosion potential (E_{cor}) was monitored during exposure tests conducted for 7-15 days.

EIS tests were carried out at 10 mV amplitude and frequencies between 20-10 kHz and 10^{-3} Hz. Spectra were obtained every 5-10 hours.

3 Results

3.1 Microstructures

During DMLS process, the laser beam intensity was modulated for ensuring the melting of the new layer of powder and slight penetration in the previous layer in order to achieve a good link between layers (wetting the layer underneath). The metallographic microstructures that arise were extensively described in a previous work (Manfredi et al. 2013), correlating them to the choice of the scanning strategy. Figure 3 reports metallographic sections along planes perpendicular and parallel to the building direction.

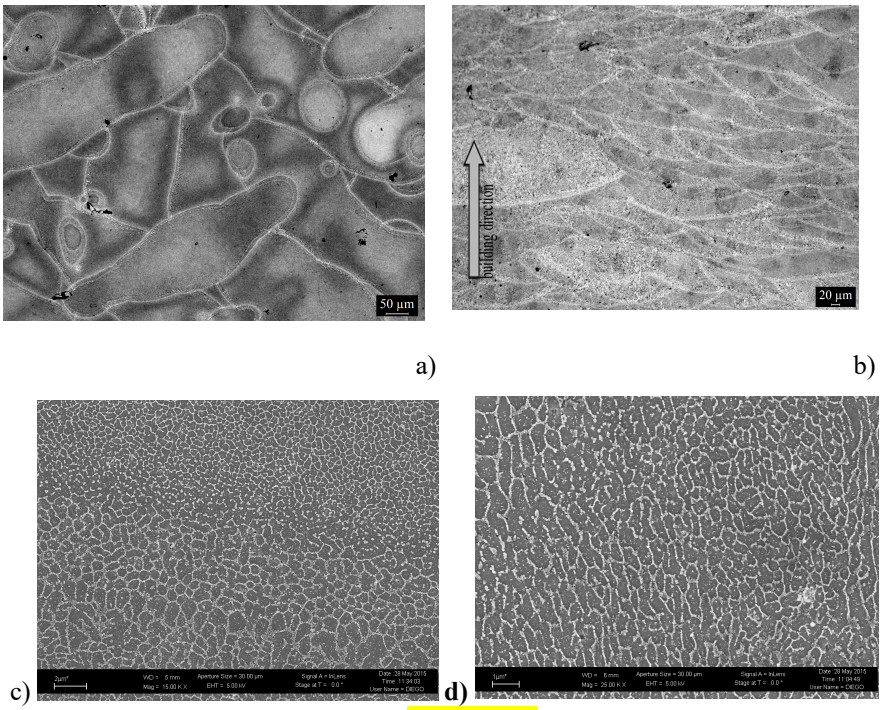

Figure 3: Microstructures of DMLS Al-10Si-Mg alloy (after etching): a) xy-plane (building direction perpendicular to this section), b) plane along z axis (or building direction, indicated by the grey arrow), c) SEM image of XY plane and d) XZ plane, showing the very fine size of the silicon crystals

The microstructure shows tracks of the scan laser during the building of the sample. Because the melting occurs in powder layer forming small melt pools, which rapidly solidify, the resulting solid microstructures achieve directional growth features far from equilibrium. The melt pools have half – cylindrical shape with dimensions (width and depth) dependent on laser power and scan spacing. Along z-direction, the macrostructure shows trace of powder deposition plane. Over the powder deposition plane, the melt pool contour lines create irregular geometric figures with the main length of melt pool that changes with the direction of laser scan, which rotates of 67° between consecutive layers. SEM analysis reveals very fine cellular grain of α-Al and Si particles with very fine size, smaller than 500 nm, in the melt pool borders (figure 3c).

Irregular pores are located at melt pool boundaries, with maximum dimension of 30 µm, due to un-melted power or insufficient overlapping between scan tracks. Near spherical pores lower than 25 µm diameter could result from entrapped gas.

3.2 Corrosion potential

Figure 4 shows the evolution of corrosion potentials during early period of immersion in the diluted Harrison's solution. The initial corrosion potential depends on surface finishing.

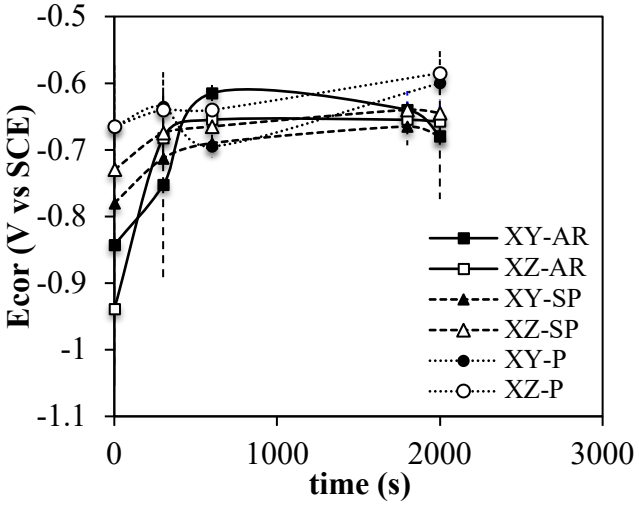

Figure 4: evolution of free corrosion potentials of DMLS Al Si10Mg alloy during initial period of exposure in diluted Harrison's solution

The specimens with rough AR surface show very negative initial values - close to -0.85 and -0.95 V vs SCE - before reaching stable values measured on polished surface (P), after just ten minutes of exposure. Shot peened surfaces (SP specimens) show similar behaviour, but with less negative early values. After half an hour of immersion, all the specimens show corrosion potentials between -0.7 mV and -0.6 V vs SCE, comparable with polished specimens (P). After 300-500 hours, the corrosion potential of the specimens became constant in the range -0.6 to -0.65 V vs SCE for the AR specimens and -0.65 to -0.69 V for the SP specimens.

3.3 Potentiodynamic tests

Figure 5 and Figure 6 show the typical trend of potentiodynamic curves on specimens with different building directions.

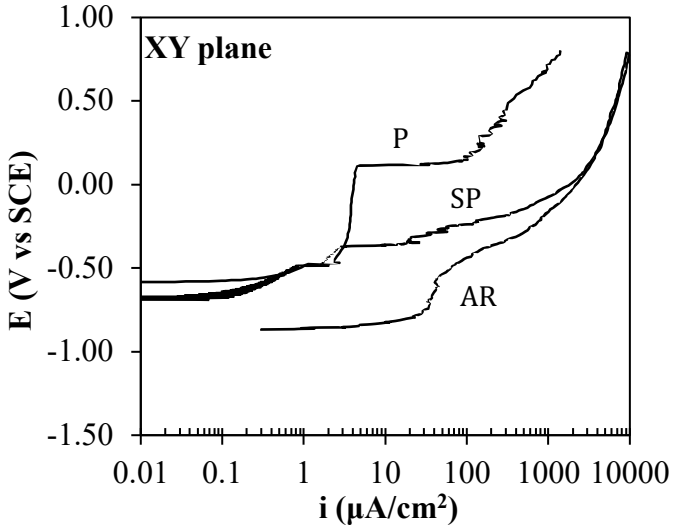

Figure 5: potentiodynamic curves on DMLS Al Si10Mg alloy in diluted Harrison's solution on XY specimens with different finishing

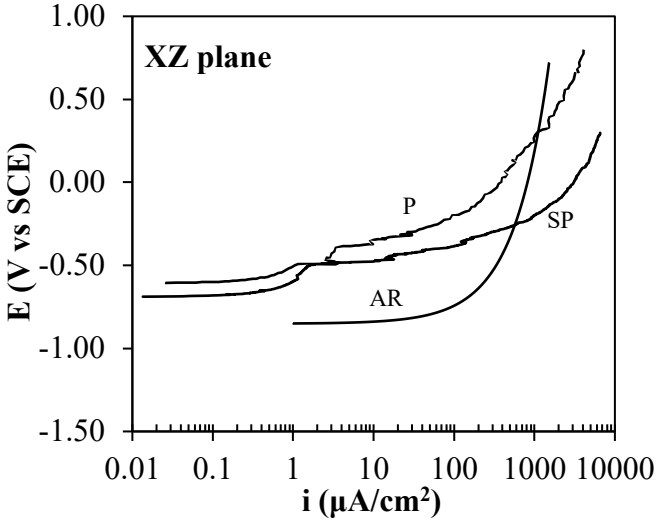

Figure 6: potentiodynamic curves on DMLS Al Si10Mg alloy in diluted Harrison's solution on XZ specimens with different finishing

Superficial porosities and roughness significantly affect the potentiodynamic curves and very scattered results were observed. The roughness decreases one order of magnitude from AR to SP specimens, from 23 µm to 4 µm of mean value (Calignano et al. 2013). For both these surface conditions, it is much higher than polished specimens, where it is possible to reach values of about 0.1 µm.

The curves on AR surfaces show a like-active behaviour with a very narrow passivity just above corrosion potential. On the contrary, wide passivity range was observed on P specimens, on xy-plane, but with large variability of pitting potentials (E_{pit}) from -0.4 to 0.2 V vs SCE. SP specimens show intermediate behaviour.

Figure 7 reports average values, the maximum and minimum values of pitting potentials estimated by five and seven potentiodynamic tests for AR condition on xy- and xz-planes respectively, and by three or four tests for the other surface conditions and plane orientations.

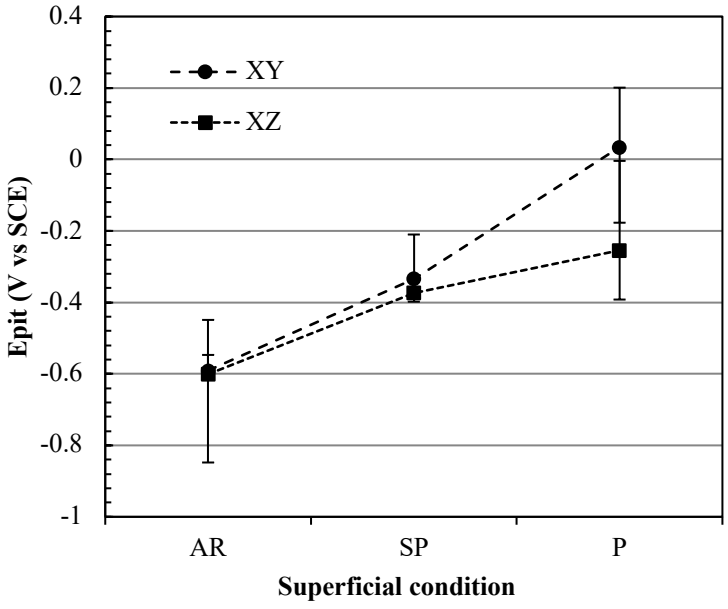

Figure 7: effect of surface finishing on pitting potential in diluted Harrison's solution of DMLS Al Si10Mg alloy. For the specimens that showed an active behaviour (like the XZ-AR in figure 6) as pitting potential was considered the free corrosion potential. In all cases the corrosion morphology was never pitting, but selective dissolution of α-Al phase on AR surface and a penetrating selective attack on the border of the melt pools inside the porosity of P and SP samples (figure 8-13).

It can be clearly noted that pitting potential increases as the surface condition changes from AR rough surface, to shot peened and polished. Minor variations can be attributed to plane orientation. As a matter of fact, XY specimens showed average pitting potentials nobler than XZ specimens.
Differences can be clearly evidenced by scanning electron microscope observations. The rough surface of AR specimens after the potentiodynamic test remains similar to that before the test (Figure 8), without any relevant pitting attack (Figure 9 and Figure 10). Selective corrosion over the whole surface was noticed at high magnification (Figure 11).

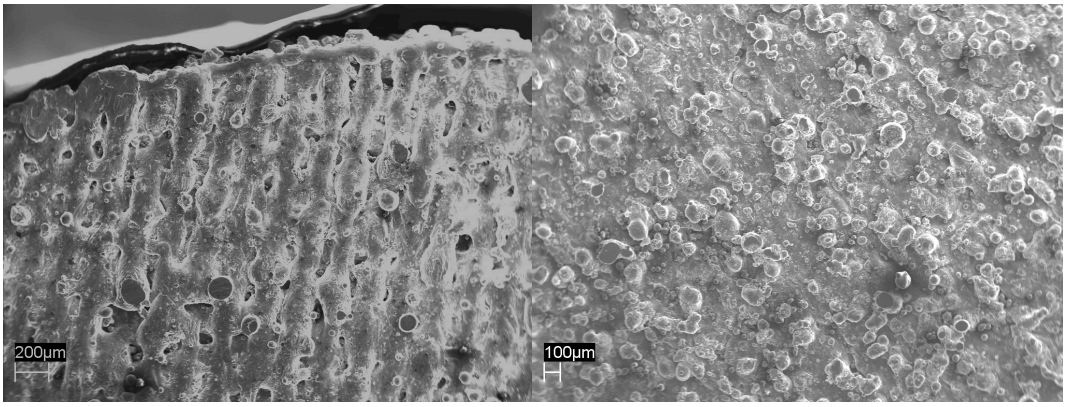

a) b)

Figure 8: SEM image at low magnification of AR surfaces of DMLS Al-10Si-Mg alloy after the potentiodynamic test (a) specimen XY (b) specimen XZ

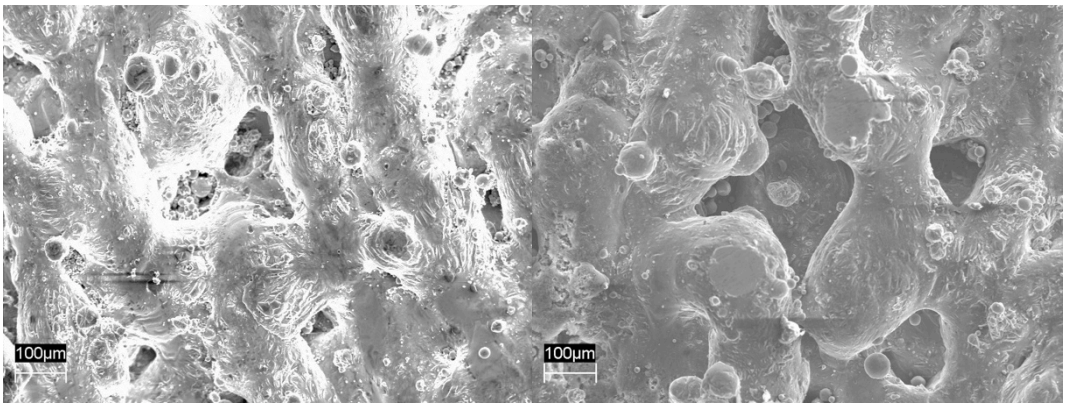

a) b)

Figure 9: SEM image of AR xy-surface of DMLS Al-10Si-Mg alloy: (a) before and (b) after the potentiodynamic test

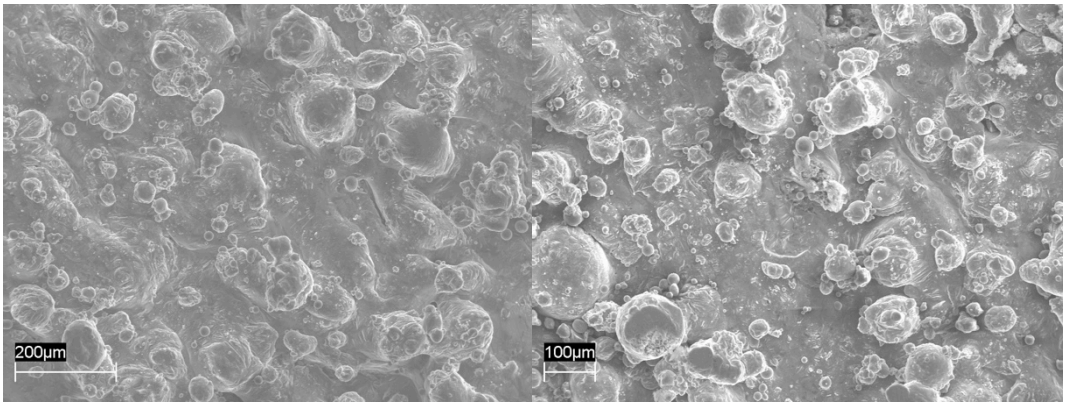

a) b)

Figure 10: SEM images of AR xz-surface of DMLS Al-10Si-Mg alloy: (a) before and (b) after potentiodynamic test

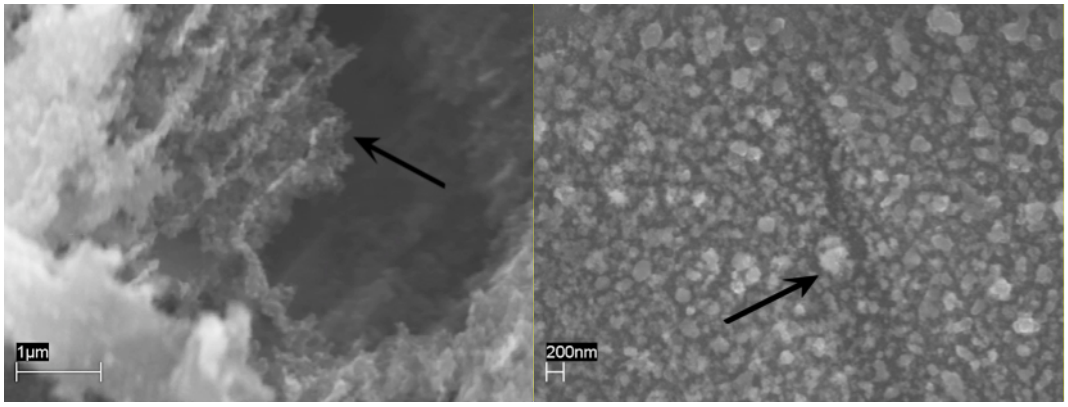

a) b)

Figure 11: high magnification close up of the specimens of figure 9 and 10 after potentiodynamic test; localized corrosion that evidences the silicon enriched dendrites inside porosity a) lateral view in XY specimen; b) overhead view on XZ specimens. The arrows indicate the silicon crystals (white in the photo). On the XZ specimen, the silicon crystals enriched all the examined area

Shot peening causes plastic deformation of edge of the original surface produced by the DMLS, giving smooth hardened areas and partial sealing of surface porosities (compare Figure 12 with Figure 9 and Figure 10).

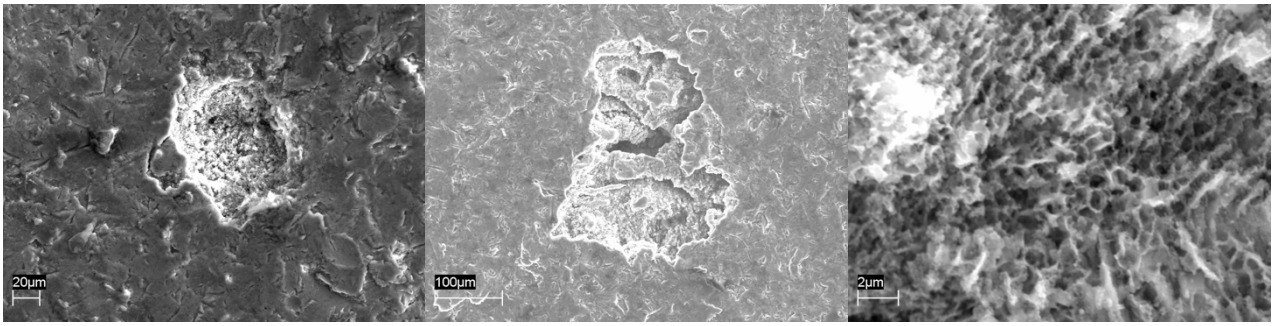

a) b) c)

Figure 12: SEM images of shot peened surfaces of DMLS Al-10Si-Mg alloy after potentiodynamic tests: (a) xy-surface, (b) xz-surface, (c) close up of the selective attack inside the pit (the withe areas are the corrosion products mainly constituted by alumina).

In a previous work, Manfredi et al (Manfredi et al. 2013) found a decrease of surface porosities from 3.3% of AR rough surface to 2.0% of shot peened surface. However, the residual porosities act as preferential sites for localized attack initiation (Figure 13) with the selective attack that can be noted inside the pit.

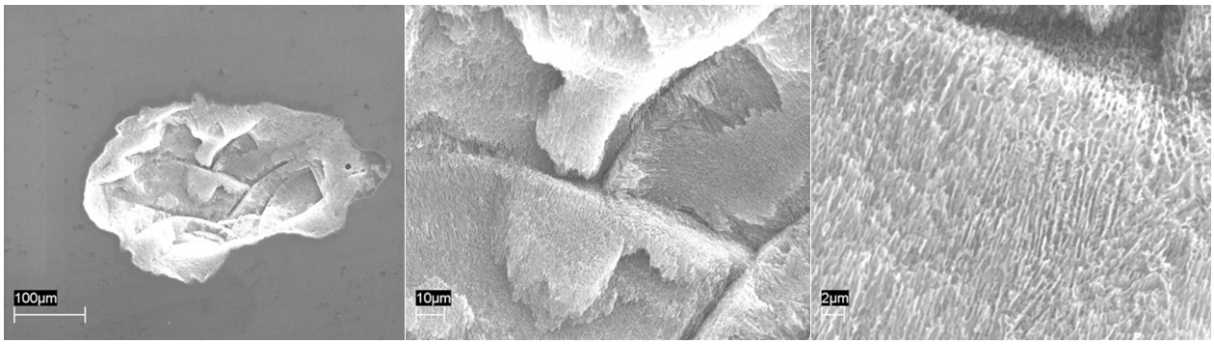

a) b) c)

Figure 13: SEM images of polished surfaces of DMLS Al-10Si-Mg alloy after potentiodynamic tests: (a) macro-image of residual surface porosities on xz specimen, (b) and (c) close up of internal surface of pore

The aluminium oxide film is quickly formed at any temperature as soon as the metal comes in contact with air. The kinetic does not depend upon the oxygen partial pressure and the temperature acts only on the final thickness. Thermal heat treatments, as the stress relieved at 300°C, modify the passive film morphology. They increase layer thickness and crystallinity of the oxide, but also produce a porous and micro-cracked structure, which have lower corrosion resistance compared to the amorphous film.

Polishing completely removes the roughness and the oxide thermally formed on the original AR surface, favouring the formation of less defective aluminium oxide film.

The residual porosities reduce to 1.1% (Manfredi et al. 2013), but even at this level they acts as preferential sites (figure 13 a). In addition, selective corrosion can be recognized along melt pools boundary inside the pit (figure 13 b and c). The polishing improves the corrosion resistance of DMLS components but it is laborious and impracticable over complex shape. However, it is not able to avoid the initiation of selective corrosion because it cannot eliminate the porosities.

3.4 EIS tests

The Bode diagram on AR XY specimen just immersed in the diluted Harrison's solution (Figure 14) shows values of the absolute value of impedance, between 10^{-3} and 10^{-1} Hz, close to 10^5 Ωcm^2. that means a slow and controlled kinetics of the corrosion process. At high frequencies, the resistance is that of the electrolyte solution, which remains constant during the test. With increasing immersion time, the absolute value of impedance at low frequencies decreases. After 150 hours of immersion, the absolute value of impedance reaches value slightly greater than 10^4 Ωcm^2.

The phase vs frequency diagrams are characterised by one wide and well-defined capacitive peak in the frequency range between 10^2 and 10^{-1} Hz for the just immerged specimens. At longer exposures, the behaviour becomes more complex and two partially overlapped peaks appear in the phase Bode plot, typical of an equivalent circuit having two time constants in this frequency range. At very low frequency, inductive behaviour was noticed, as well evidenced by the shift of the phase angle to positive values (figure 14). In the range of intermediate frequencies is possible to evidence two well defined time constants.

The behaviour of the just immerged specimens is typical of passive aluminium, and can be conveniently described by the equivalent circuit proposed by Bessone et al. (figure 15) (Bessone et al. 1992). The circuit is based on a parallel of a capacitance C1 with a series of an R1-L1 circuit and Z_T, which is a function derived for a diffusion controlled process within a finite length.

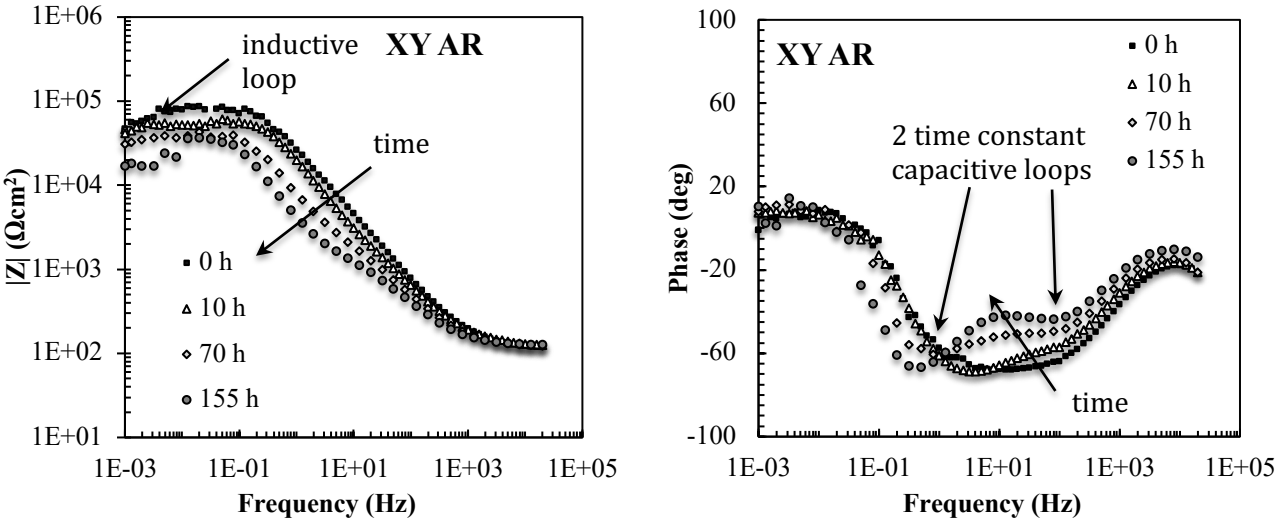

Figure 14: evolution of Bode plots on XY AR DMLS Al Si10Mg alloy in diluted Harrison's solution

The interpretation of inductive loop was discussed in several corrosion studies (aluminium alloy and aluminium based composites) but it is still controversial. Katkar et al considered partially or totally active behaviour of boron carbide composites in seawater having inductive arcs at low frequency (Katkar et al. 2011). Peng et al (Peng et al. 2010), referring to the works of Keddam et al (Keddam et al. 1997), indicated that the inductive loop is likely promoted by the weakening of the protective aluminium oxide layer. Finally, the high frequency capacitive loop could be consequent to the sealing effect of corrosion products in the porosity and in the active areas (Figure 14) whereas the behaviour at very low frequency represents the diffusion through corrosion product and inside the localized attacks.

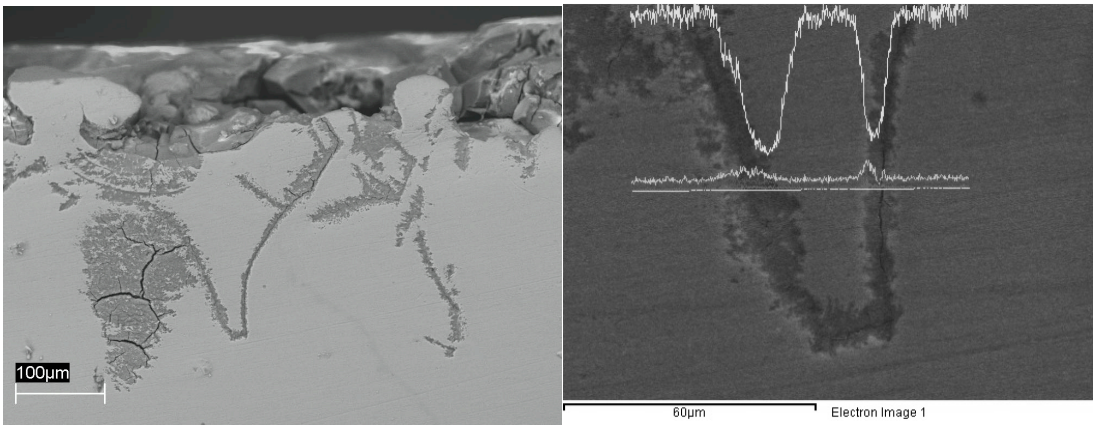

Figure 14: SEM images of selective attack on metallographic sections of XY-AR surface of DMLS Al Si10Mg alloy of after EIS monitoring and EDS line profile

The evolution of Bode diagram on XZ AR surface is similar to that described for XY-AR specimens, but the absolute value of impedance at low frequencies just after immersion is lower, indicating higher corrosion rates. The absolute value of impedance are close to XY specimens for longer exposures(Figure 17).

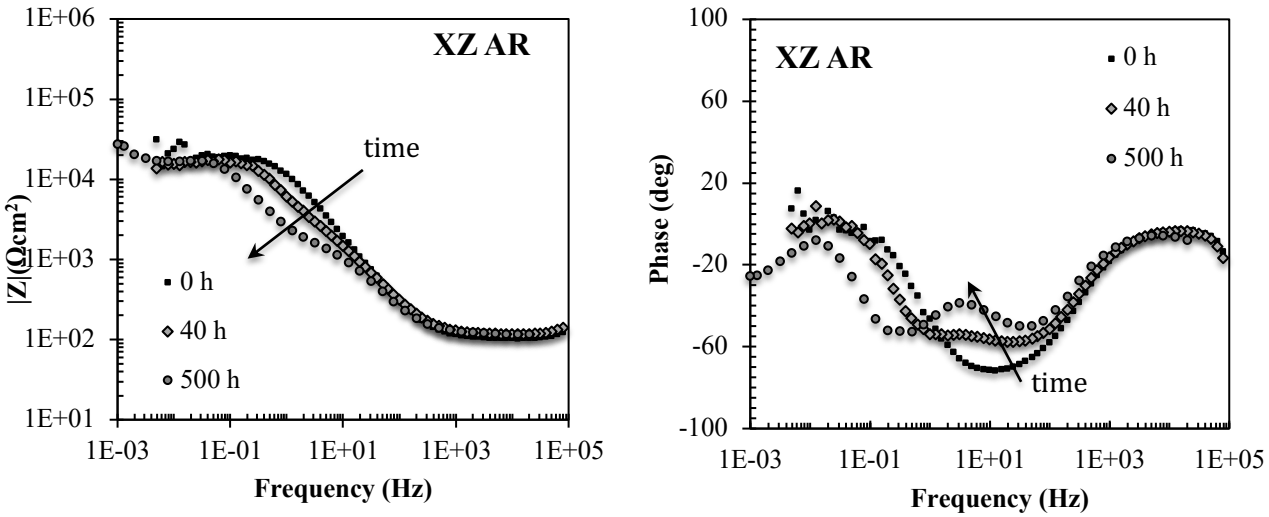

Figure 15: evolution of Bode plots on XZ AR DMLS Al-10Si-Mg alloy in diluted Harrison's solution

A similar behaviour was observed on the shot peening and polished specimens. The evolution of Bode plots of polished XY specimens are reported in Figure 18.

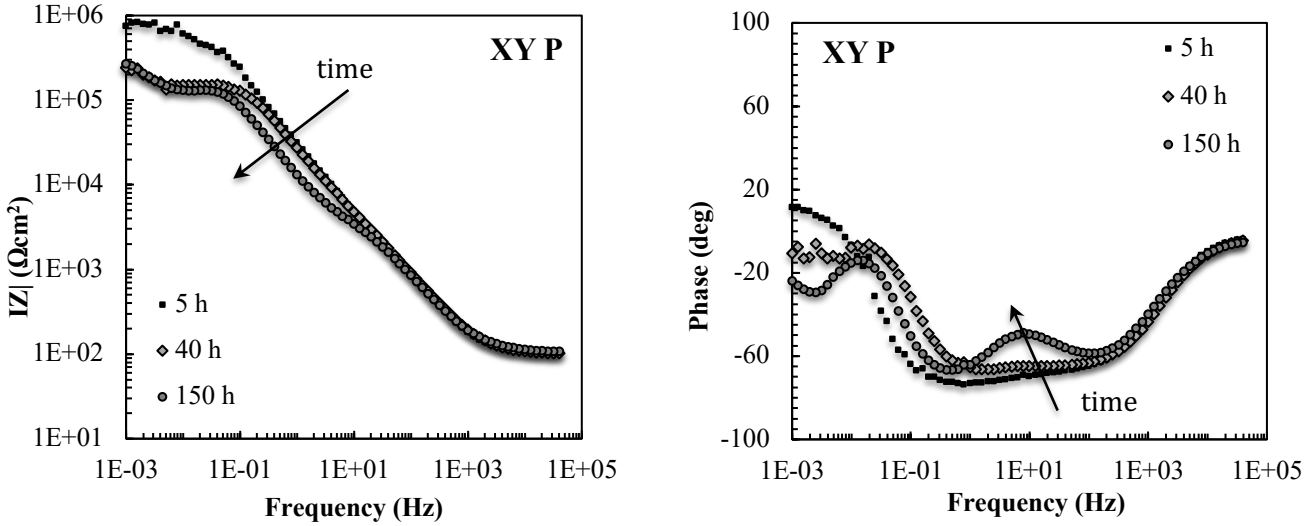

Figure 16: evolution of Bode plots on P XY DMLS Al Si10Mg alloy in diluted Harrison's solution

The absolute value of impedance at low frequencies decreases at longer exposures, up to one order of magnitude at the end of the test. Specimens exposed more than 40 hours, in the range of intermediate frequencies, showed the presence of a second very well defined time constant.
Figure 19 summarizes the effect of surface finishing on the EIS spectra measured after 5-6 hours of immersion.

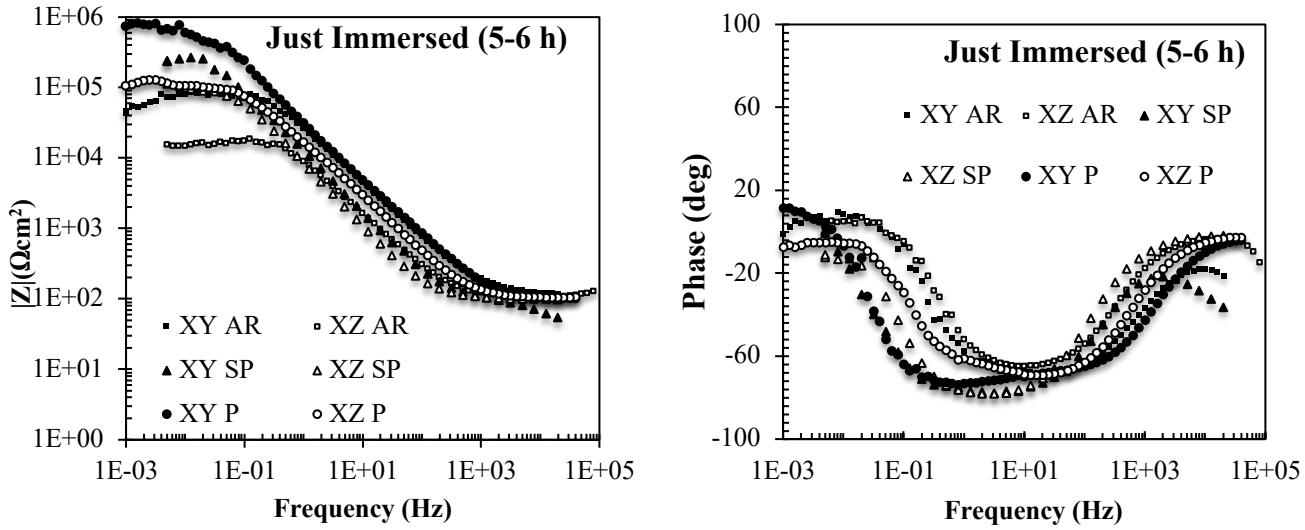

Figure 17: Effect of surface finishing for just immersed specimens (Bode plots)

Polished specimens - which tend to form a stable passive film - have higher absolute values of impedance at low frequency than shot peened ones, and much more high modules than as received specimens for same building directions. For same surface finishing, XY specimens always show a better corrosion behaviour than XZ. At high frequencies, the absolute values of impedance of all the specimens are very close and correspond to the resistance of the electrolyte solution. After about 200 hours, the corrosion behaviour of AR, SP and P specimens are similar.
SEM analysis at the end of EIS monitoring confirmed that corrosion occurred along preferential path (Figure 16), with selective attacks at the melt pool borders. The EDS analysis was not able to point out differences in composition of the individual particles due to their small size. However, an enrichment of silicon and oxygen in correspondence of the etched areas was found (Figure 16 b).

4 Discussion

The results point out that the corrosion resistance of aluminium alloys produced by DMLS mainly depends on the rough and porous surface produced by the process, the insurgence of selective attacks and the formation of an oxide film less protective than the passive film that usually forms on aluminium. The different density of surface porosities and high concentration of the melt pool borders over the XZ surface produce a different corrosion behaviour respect to XY surface.
The AR specimens showed a near active behaviour during potentiodynamic tests and EIS analysis. The selective attack occurs predominantly in the transition zone between the laser tracks. The selective dissolution of α-Al phase is due to the nobility of silicon particles respect to aluminium (Liang et al. 2013) and (Zhou et al. 2008). The microstructure of Al-10Si-Mg specimens obtained by DMLS is extremely fine and quite different from that observed after casting. The metallographic analysis confirms a microstructure that reflects the tracks of fusion (Aboulkhair et al. 2014). Several authors have studied the microstructure within these tracks both on eutectic and hypoeutectic Al-Si alloys. Brandl et al. reported that the as-built microstructure is characterised by cellular dendrites of a-Al and the interdendritic Si-particles (Brandl et al. 2012). α-Al phase solidification takes place in the melt pool in cellular grains of different size, changing with the location from center to edge of each individual track (Thijs et al. 2013). Due to the very fast solidification, the α-Al phase remains supersaturated and the residue silicon segregates at grain boundaries (Prashanth et al. 2014). According to Thijs et al (Thijs et al. 2013), silicon crystallizes in the form of fibrous particles that decorates the primary α-Al cellular grains. This structure can be defined as intercellular network of silicon. The network is interrupted in the heat affected zone (HAZ) just placed below two tracks

overlap. In this zone, the silicon particles become coarser and with idiomorphic crystals, due to the increase of diffusivity of silicon during heating. Osòrio et al reported the corrosion rate of two cast Al alloys containing 5% and 9% Si, respectively. The rate increases with decreasing size of the grains. This was associated with very fine distribution of eutectic silicon particles. Furthermore, the raise of silicon concentration in the alloy increases the fraction of eutectic, giving higher corrosion rates (Osòrio et al. 2008). Pech-Canul et at also reported the preferential dissolution of Mg from the Mg_2Si intermetallic in chlorides solution (Pech-Canul et al. 2012). This could explain the preferential corrosion observed in the HAZ of the melt tracks, in which silicon is principally present as a separate phase and not in oversaturated solid solution.
During the DMLS process, a film of oxide forms, but it is less protective than the spontaneous film that covers aluminium in air. This can be ascribed to different aspects. DMLS process is performed in argon atmosphere, which is very poor in oxygen. Argon is an inert gas. Thus, it is not suitable to bind chemically to the surface, but it could be trapped and embedded in the superficial film during the rapid solidification, influencing its continuity. Actually, the presence of argon on the surfaces of the specimens was also determined with the EDS microprobe. According to Olakanmi (Olakanmi 2013), the surface of the powders is strongly oxidized. Parts of aluminium oxide initially present on the metallic powder, which is crushed by the heat of the laser, could also be accumulated over the surface. Isolated particles of aluminium oxide, coming from powder, could inhibit the correct reformation of a continuous film on the surface, interfering with the correct repassivation of aluminium.
Furthermore, despite DMLS process works in an inert atmosphere, the gas can usually contains 0.1-0.12% residual oxygen and oxidation can even occur. The presence of Al oxides formed during DMLS process was also noted by Louvis et al (Louvis et al. 2011). They concluded that the power of the laser should be high enough to break through the oxide layer formed on the top of deposited tracks. The power of the laser used for DMLS process is enough to smash the oxide film, which is incorporated in the transition zone of the merged drops after each pass.
Mechanical actions of shot peening smooth the original rough surface and remove the film formed during DMLS process surface and permit the correct formation of protective oxide to form. The surface roughness decreases about one magnitude order but not all film formed during DMLS process is removed and the surface exposed to the aggressive environment is not entirely covered by the best protective oxide.
The specimens with surface polished up to 0.1 μm alumina powder showed higher corrosion resistances. Unfortunately, the polishing still leaves porosities on the surface. Inside these porosities, the surface remains unaltered, making the porosities a preferential site for localized corrosion. Thus, apparent corrosion current density and pitting potential depend on the numbers and on the dimensions of the emerging porosities.

5 Conclusions

The corrosion behaviour of DMLS Al-10Si-Mg alloy was studied in order to establish the effect of surface finishing and the building direction.
Roughness, surface porosities and the presence of less protective superficial film formed during process significantly worsen the corrosion behaviour of the DMLS alloy. The corrosion resistance increases from rough surface formed during the process to the smoothed shoot peened surface to polished one.
The texture of melting tracks reduces corrosion resistance of the surfaces parallel to the building direction, because of the high density of melting tracks borders.
A selective corrosion of α-Al in the border of the melting tracks was observed. It results from the enhanced content of silicon in the solid solution in the melt pool due to the rapid solidification and cooling that increases corrosion resistance, and the formation of preferential dissolution path in HAZ of pool where silicon particles separate as idiomorphic crystals and galvanic couple takes place.

References

Aboulkhair, NT, Everitt, NM, Ashcroft, I & Tuck, C 2014, 'Reducing porosity un AlSi10Mg parts processed by selective laser melting', *Additive Manufactoring*, vol 1, no. 1-4, pp. 77-86.

Andreatta, F, Terryn, H & de Wit, 2003, 'Effect of solution heat treatment on galvanic coupling between intermetallics and matrix in AA7075-T', *Corrosion Science*, vol 45, no. 8, pp. 1733-1746.

Büchler, M, Watari, T & Smyrl, WH 2000, 'Investigation of the initiation of localized corrosion on aluminium alloys by using fluorescence microscopy', *Corrosion Science*, vol 42, pp. 1661-1668.

Battocchi, D, Simoes, AM, Tallman, DE & Bierwagen, GP 2006, 'Comparison of testing solutions on the protection of Al-alloys using a Mg-rich primer', *Corrosion Science*, vol 48, pp. 2226–2240.

Brandl, E, Heckenberger, U, Holzinger, V & Buchbinder, D 2012, 'Additive manufactured AlSi10Mg samples using Selective Laser Melting (SLM): Microstructure, high cycle fatigue, and fracture behaviour', *Materials and Design* , vol 34, pp. 159-169.

Calignano , F, Manfredi , D, Ambrosio , EP, Iuliano , L & Fino, P 2013, 'Influence of process parameters on surface roughness of aluminium parts produced by DMLS ', *International Journal of Advanced Manufuctoring Technologies*, vol 67, pp. 2743–2751.

Cao, CN, Wang, J & Lin, HC 1989, , *Journal of Chinese Society of Corrosion Protection*, vol 9, p. 261.

Davis, J 1998 , *Metals Handbook Desk Edition*, ASM International.

Fratila-Apachitei, LE, Apachitei, I & Duszcz, J 2006, 'Characterization of cast AlSi(Cu) alloys by scanning Kelvin probe force microscopy', *Electrochimica Acta*, vol 51, pp. 5892–5896.

Fulcher, BA, Leigh, DK & Watt, TJ 2014, 'Comparison of AlSi10Mg and Al 6061 Processed Through DMLS', *In Proc. Solid Freeform Fabrication (SFF) Symposium*, Austin, Texas.

Guillaumin, V & Mankowski, G 2000, 'Localized corrosion of 6056 T6 aluminium alloy in chloride media', *Corrosion Science*, vol 42, no. 1, pp. 105-125.

Katkar, VA, Gunasekaran, G, Rao, AG & Koli, PM 2011, 'Effect of the reinforced boron carbide particulate content of AA6061 alloy on formation of the passive film in seawater', *Corrosion science*, vol 53, pp. 2700-2712.

Keddam, M, Kuntz, H, Takenouti, D, Schuster, D & Zuili, D 1997, 'Exfoliation corrosion of aluminium alloys examined by electrode impedance', *Electrochimica Acta* , vol 42, no. 1, pp. 87-97.

Liang, ZX, Ye, B, Zhang, L, Wang, QG, Yang, WY & Wang, QD 2013, 'A new high-strength and corrosion resistant Al-Si based casting alloy', *Materials Letters* , vol 97, pp. 104-107.

Louvis, K, Fox, L & Sutcliffe, CJ 2011, ' Selective laser melting of aluminium components', *Journal of Materials Process Technologies*, vol 211, pp. 275-284.

Manfredi, D, Cagliano, F, Ambrosio, EP, Krishnan, M, Canali, R, Biamino, S, Pavese, M, Atzeni, E, Iuliano, L, Fino, P & Badini , C 2013, 'Direnct Metal Laser Sintering: an additive manufacturing technology ready to produce lightweight structural parts for robotic applications', *La metallurgia italiana* , vol 105, no. 10, pp. 15-24.

Manfredi, D, Calignano, F, Manickavasagam, K, Canali, R, Ambrosio, EP & Atzeni, E 2013, 'From powders to dense metal parts: characterization of a commercial AlSiMg alloy processed through direct metal laser sintering', *Materials*, vol 6, pp. 856-869.

Merceis, P. and J-P. Kruth. 2006. Residual stresses in selective laser sintering and selective laser melting. *Rapid Prototyping Journal*. 12(5), pp.254-265. Miller, WS, Zhuang, L, Bottema, J, Wittebrood, AJ, De Smet, P, Haszler, A & Vieregge, A 2000, 'Recent development in aluminium alloys for the automotive industry,', *Materials Science and Engineering A* , vol 280, no. 1, pp. 37-49.

Olakanmi, EO 2013, 'Selective laser sintering/melting (SLS/SLM) of pure Al, Al–Mg, and Al–Si powders: Effect ofprocessingconditionsandpowderproperties ', *Journal of Materials Processing Technology*, vol 213, pp. 1387-1415.

Osòrio, WR, Goulart , PR & Garcia, A 2008, 'Effect of silicon content on microstructure and electrochemical behaviour of hypoeutectic Al.Si alloys', *Materilas Lettes*, vol 62, pp. 365-369.

Pech-Canul, MA, Pech-Canul, MJ, Guevara Vela, JM, Ugalde Saldívar, VM, Aguilar, JC & Coral-Escobar, EE 2012, 'Corrosion Characteristics of an Al-17%Si-14%Mg Alloy in Chloride Solutions', in *Recent Developments in Metallurgy, Materials and Environment*, Cinvestav IPN, Unidad Saltillo, Mexico.

Peng, GS, Chen, KH, Fang, HC, Chao, H & Chen, SY 2010, 'EIS study on pitting corrosion of 7150 aluminium alloy in sodium chloride and hydrochloric acid solution', *Materials and Corrosion*, vol 61, no. 9, pp. 783-789.

Prashanth, KG, Scudino, S, Klauss, HJ, Surreddi, KB, Lober, L, Wang, Z, Chaubey, AK, Kuhn, U & Eckert, J 2014, 'Microstructure and mechanical properties of Al-12Si producd by selective laser melting: effect of heat treatment ', *Materials Science & Engineering A* , vol 590, pp. 153-160.

Read, N, Wang, W, Essa, K & Attallah, MM 2015, 'Selective laser melting of AlSi10Mg alloy: Process optimisation and mechanical properties development', *Materials and Design*, vol 65, pp. 417–424.

Shiomi, M., K. Osakada, K. Nakamura et al. 2004. Residual stress within metallic model made by selective laser melting process. *CIRP Ann—Manuf Technol*. 53(1), pp.195–198.

Sun, Y, Moroz, A & Alrbaey, K 2014, 'Sliding Wear Characteristics and Corrosion Behaviour of Selective Laser Melted 316L Stainless Steel', *Journal of Materials Engineering and Performance*, vol 23, no. 2, pp. 518-526.

Szklarska-Smialowska, Z 1999, 'Pitting corrosion of aluminium', *Corrosion Science*, vol 41, no. 9, pp. 1743-1767.

Thijs, L, Kempen, K, Kruth, J-P & Van Humbeeck, J 2013, 'Fine-sructured aluminium products with controllable texture by selective laser melting of pre-alloyed AlSi10Mg powder', *Acta Materialia* , vol 61, pp. 1809-1819.

Wei, RP, Liao, C & Gao, M 1998, 'A transmission electron microscopy study of constituent-particle-induced corrosion in 7075-T6 and 2024-T3 aluminium alloys', *Metallurgical and Materials Transactions A: Physical, Metallurgy and Materials Science*, vol 29, no. 4, pp. 1153-1160.

Zaeh M, Branner G. Investigations on residual stresses and deformations in selective laser melting. Prod Eng 2010;4(1):35–45

Zhou, W, Aung, NN, Choudharybc, A & Kanounic, M 2008, 'Heat-transfer corrosion behaviour of cast Al alloy', *Corrosion Science*, vol 50, pp. 3308–3313.